incident pion ($\sim 20\%$ of the events). With modest restrictions of the four-momentum transfer ranges, the data are well described by a double-Regge approximation where the nondiffractive vertices are represented by a constant residue and a pole. Phase space is separated into two regions, each of which is assumed to be dominated by one exchange diagram; thus the model can be applied without high-mass restrictions, and double counting in the sense of duality is avoided. Since each region was independently well described by the model, the data for each distribution can be summed over the two regions spanned and can maintain the quality of the description if the diagrams are added incoherently.[10]

The low-mass enhancement in the A region is effectively reproduced by the amplitudes in the t channel corresponding to diagrams a-I and a-II as suggested by semilocal duality.

PHYSICAL REVIEW D VOLUME 2, NUMBER 7 1 OCTOBER 1970

A Study of the $K\pi\pi$ System in $K^-p \to K^-\pi^+\pi^-p$ at 12.6 GeV/c*

T. Ludlam, J. Sandweiss, and A. J. Slaughter
Yale University, New Haven, Connecticut 06520
(Received 15 June 1970)

The $K\pi\pi$ spectrum in the reaction $K^-p \to K^-\pi^+\pi^-p$ at 12.6 GeV/c is analyzed, taking as a starting point the observation that the transverse momentum distributions are uniform throughout this spectrum and are restricted to small values. This behavior results in a threshold enhancement in the $K\pi\pi$ spectrum corresponding to every $K\pi$ mass value. With the exception of the Q peak, and perhaps the L meson, the $K\pi\pi$ mass spectrum can be regarded as a continuous sequence of such enhancements, which follow from phase-space distributions in the longitudinal momenta. A double-Regge-pole-exchange model for the Q gives qualitative agreement with the data, but only if at least two exchange amplitudes are included; it does not give a correct description of the detailed correlations between the longitudinal and transverse momenta. A more successful description is given by a very simple resonance model. The similarities between the predictions of these two models—which are related by the concept of duality—are discussed in terms of the kinematic restrictions imposed by the condition of small transverse momenta.

I. INTRODUCTION: SOME CHARACTERISTIC FEATURES

RECENTLY, experimenters with high-energy bubble-chamber data have devoted considerable attention to threshold boson enhancements in reactions like

$$M+T \to (M\pi\pi)+T\,, \tag{1}$$

where M represents an incident meson and T a nucleon target. The threshold enhancements in the $M\pi\pi$ system result, presumably, from diffraction dissociation of the incident beam particle, and are seen only when two of the outgoing mesons combine to form a resonant state. For incident π mesons, the observed enhancements are A_1 ($\rho\pi$) and A_3 ($f\pi$), and for incident kaons one observes the Q ($K^*(890)\pi$; $K\rho$) and L ($K^*(1420)\pi$). In the cases of the Q and A_1, very detailed analyses of the experimental data have been performed—with considerable success—from each of two apparently divergent points of view: (i) assuming a double-peripheral t-channel exchange amplitude (Deck effect), and (ii) assuming the observed enhancements to consist primarily of peripherally produced resonant states of definite spin and parity.[1] The principle of duality, as demonstrated in the case of two-body final states by Dolen, Horn, and Schmid,[2] is usually invoked to reconcile the apparent equivalence of these two approaches in understanding the experimentally observed phenomena.

In this paper we examine the behavior of the $K\pi\pi$ system in the reaction

$$K^-p \to K^-\pi^+\pi^-p \tag{2}$$

for an incident kaon momentum of 12.6 GeV/c. The data to be discussed are from an investigation of 1291 examples of reaction (2) in an exposure of the BNL 80-in. bubble chamber to a beam of 12.6-GeV/c rf-separated K^- mesons. The $K^-\pi^+$ and $K\pi\pi$ mass spectra for this reaction are shown in Fig. 1. In Fig. 1(a), the $K^*(890)$ peak is seen to dominate the reaction. A small $K^*(1420)$ peak is also present. The $K\pi\pi$ spectrum has as its most obvious feature the Q peak, which re-

* This work [Yale Report No. 2726-580 (unpublished)] is supported by the U. S. Atomic Energy Commission under Contract No. AT(30-1)2726. The authors hold guest appointments at Brookhaven National Laboratory, Upton, New York.

[1] A recent review of the analysis of the Q and A_1 peaks, with extensive references, is given by M. Derrick, in *Proceedings of the Boulder Conference on High-Energy Physics*, edited by K. T. Mahanthappa, W. D. Walker, and W. E. Brittin (Colorado A.U.P., Boulder, 1970), p. 291. Some controversy exists as to whether the L meson is entirely the result of threshold production of $K^*(1420)+\pi$. See the review by C. Y. Chien, in Johns Hopkins University Report No. JHU-7010, 1970 (unpublished).

[2] R. Dolen, C. Horn, and D. Schmid, Phys. Rev. **166**, 1768 (1968); G. Chew and A. Pignotti, Phys. Rev. Letters **20**, 1078 (1968).

sults largely from threshold production of $K^*(890)+\pi$ as shown by the shaded events. The only other structure is a narrow excess of events at the mass of the L meson (approximately 1760 MeV), which has no apparent contribution from $K^*(890)$. Figure 2 shows in more detail the contribution of two-body resonant states to the $K\pi\pi$ mass spectrum. These estimates were made, in the intervals shown by the horizontal error bars, by fitting each of the two-body distributions with S-wave Breit-Wigner shapes plus a polynomial background, using a maximum-likelihood fitting program. Possible interference effects have been neglected. The $K^*(890)$, ρ, and $K^*(1420)$ signals each rise sharply just above threshold for production. (In each case the threshold mass is shown by an arrow on the horizontal scale.) Each is confined to a rather narrow region of the $K\pi\pi$ mass spectrum above this value.

One of the most striking characteristics of the data is illustrated in Fig. 3. This shows the uniform behavior of the transverse momenta for reaction (2). On the right-hand side of the figure, the average transverse momenta for the $K^-\pi^+$ system, the π^-, and the proton are plotted as a function of the $K^-\pi^+$ invariant mass. These averages remain constant at about 0.4 GeV/c throughout the $K\pi$ mass spectrum. (The total c.m.

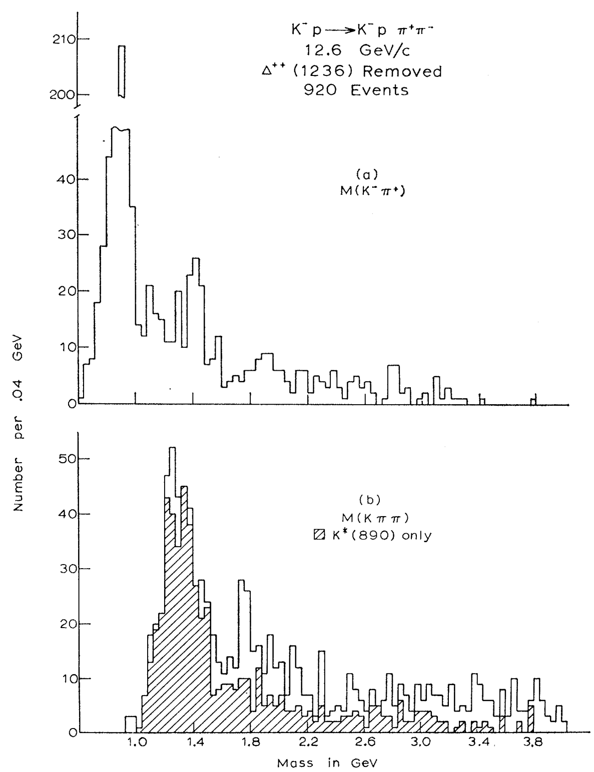

FIG. 1. (a) $K^-\pi^+$ effective-mass distribution for reaction (2). Note break in vertical scale. (b) $K^-\pi^+\pi^-$ mass spectrum. Shaded area includes events with $0.8<M(K^-\pi^+)<1.0$ GeV. In both (a) and (b), the $\Delta^{++}(1236)$ background $[1.16<M(p\pi^+)<1.32$ GeV$]$ has been removed.

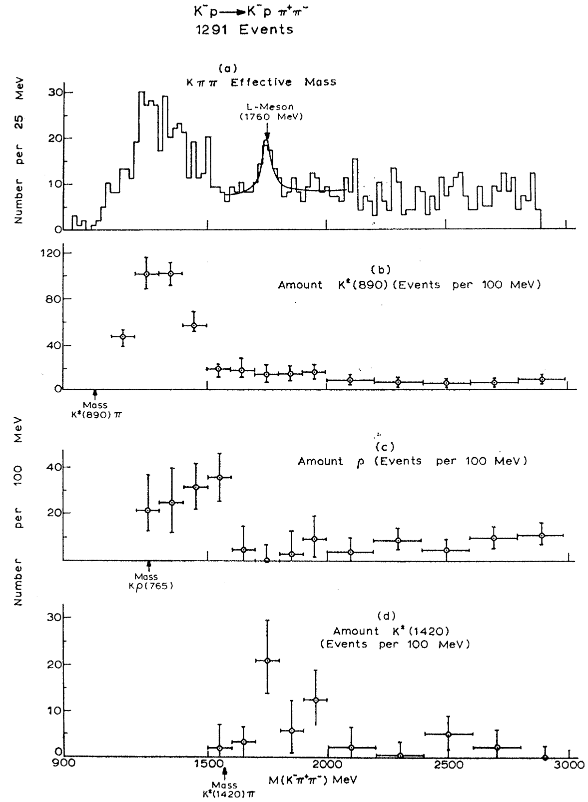

FIG. 2. Amounts of $K^*(890)$, $\rho(765)$, and $K^*(1420)$ signals as a function of the $K\pi\pi$ mass (see text). No Δ^{++} subtraction has been made. Solid curve in (a) is the result of a maximum-likelihood fit of this portion of the spectrum to an S-wave Breit-Wigner shape for the L meson plus a polynomial background. Fitted parameters are $M=1.76\pm0.015$ GeV, $\Gamma=0.05_{-0.02}^{+0.04}$ GeV.

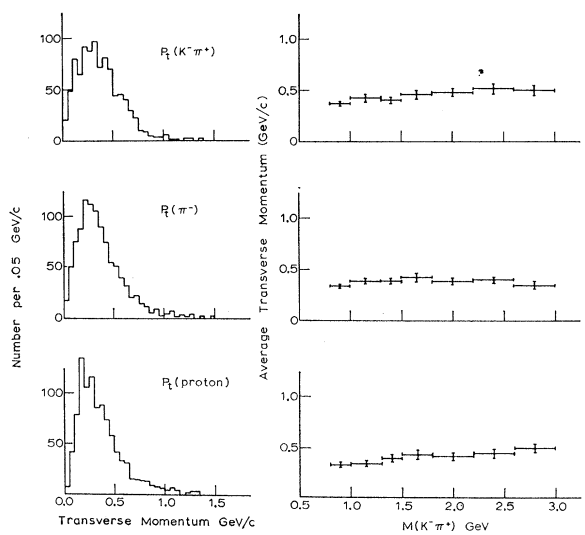

FIG. 3. Transverse momentum behavior for the reaction $K^-p \to (K^-\pi^+)\pi^-p$. Average values of the transverse momenta are plotted on the right-hand side for the $K^-\pi^+$ mass intervals indicated by the horizontal error bars. Transverse momenta are histogrammed on the left-hand side. Δ^{++} background has been removed.

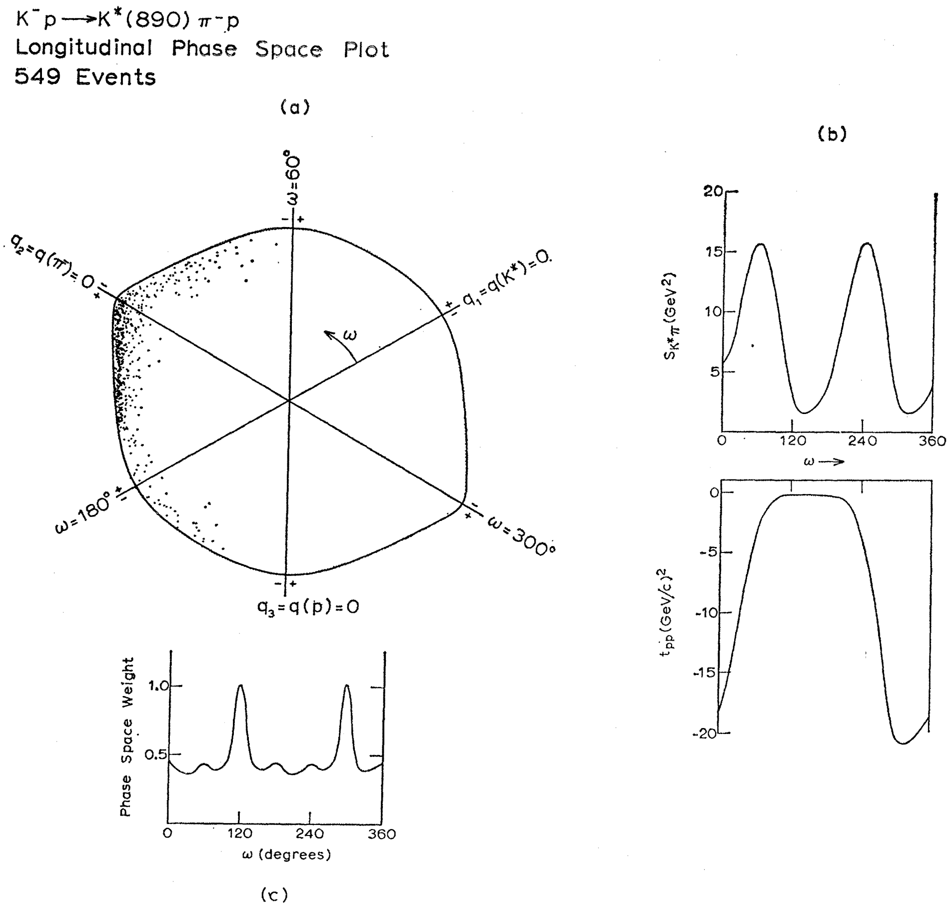

FIG. 4. (a) van Hove plot of the longitudinal momenta for events in the $K^*(890)$ peak. (b) $S_{K^*\pi}$ (the square of the $K^*\pi$ invariant mass) and t_{pp} (the squared four-momentum transfer from the incident to the outgoing proton) as functions of ω for the average transverse momenta:

$$\langle P_t(K^*)\rangle = 0.37 \text{ GeV}/c,$$
$$\langle P_t(\pi^-)\rangle = 0.34 \text{ GeV}/c,$$
$$\langle P_t(p)\rangle = 0.33 \text{ GeV}/c.$$

Curves are drawn for

$$M(K^*) = 0.89 \text{ GeV}.$$

(c) Lorentz-invariant phase-space density (for the average transverse momenta) as a function of ω. Vertical scale is arbitrary.

energy is 5.0 GeV.) Furthermore, the spread about these average values is narrow, as seen in the histograms on the left-hand side of the figure.

Examination of Figs. 1 and 2 suggests that for small values of the $K\pi\pi$ mass the behavior in the three-body spectrum results directly from a sequence of threshold enhancements in the production of two-body resonances.[3] A more general observation of this nature has been made by Barbaro-Galtieri *et al.*[4] in a study of K^+p interactions at 12.0 GeV/c: They find that *any* narrow selection on the $K\pi$ mass results in a threshold enhancement in the corresponding $K\pi\pi$ spectrum.

The purpose of this paper is to emphasize the fundamental importance of the transverse momentum behavior illustrated in Fig. 3, irrespective of its dynamic origin. We show in Sec. II that this feature alone is sufficient to describe the continuum portion of the $K\pi\pi$ spectrum which underlies the Q and L peaks of Fig. 1(b), and to explain the aforementioned observation of Barbaro-Galtieri *et al.* In Sec. III we examine in detail two hypotheses for the production of the Q peak: a double-Regge-pole-exchange model and a very simple resonance model. Both give qualitatively similar results, the resonance model giving a more accurate description of the data. We point out that the similarity between the predictions of these two models—which are related by duality—follows from the kinematic restrictions imposed by the conditions of small transverse momenta. We refer to this result as kinematic duality.

II. THE CONTINUUM: A STUDY IN LONGITUDINAL PHASE SPACE

Given the simple—and uniform—behavior shown in Fig. 3 for the transverse momenta, it seems appropriate to apply an analysis technique which isolates the longitudinal and transverse components of phase space. Such a technique has been proposed by van Hove[5]: the method of longitudinal phase-space analysis. This method is especially straightforward for the case of

[3] The contribution from $K^*(890)\pi$ and $K\rho$ in the Q region of the $K\pi\pi$ mass [$M(K\pi\pi)<1.5$ GeV] amounts, within errors, to 100% of the observed events. The rise in the $K^*(1420)\pi$ contribution at threshold corresponds to the position of the L-meson signal in Figs. 1(b) and 2(a). The conclusion that the enhancement in the $K^*(1420)\pi$ signal is entirely responsible for the observed L peak cannot be drawn with certainty from the present small statistical sample.

[4] A. Barbaro-Galtieri *et al.*, Phys. Rev. Letters **22**, 1207 (1969).

[5] L. van Hove, Nucl. Phys. **B9**, 331 (1969).

three-body final states, and so promises to be particularly appropriate for the present case of interest in view of the characteristic quasi-three-body behavior emphasized above.

The van Hove plot of the longitudinal momenta for events in the $K^*(890)$ peak is shown in Fig. 4(a). As described in Ref. 5, the plot has three axes which intersect at 60° angles. Along each of these axes the longitudinal momentum (q) of one of the three outgoing particles is zero. A given event, with longitudinal momenta q_i ($i=1, 3$), is represented by a point on this plot such that the perpendicular distance to the ith axis is q_i. The positive and negative sides of each axis are given by the $+$ and $-$ signs in the figure, the $+$ direction being along the c.m. momentum vector of the incident beam. For a given set of transverse momenta, $\mathbf{P}_{t,i}$ ($i=1, 3$), the constraint of energy conservation defines a curve on this plot along which all events with this particular set of transverse momenta must lie. The kinematic boundary in Fig. 4(a) is given by the case in which all of the transverse momenta are zero. The essential feature is that, because of the smallness of the transverse momenta, all of the points lie in a narrow band close to this boundary. Thus all of the main features of the data can be described in terms of the angular coordinate ω which, as shown in the figure, is measured counterclockwise from the axis along which $q_1=0$.

For a specific set of transverse momenta, which we take to be the experimentally determined average values, ω gives a complete description of the longitudinal configuration. All of the two-particle invariant masses and momentum transfers can be described in terms of this parameter. Two examples are shown in Fig. 4(b). Here $S_{K^*\pi}$ (the square of the $K^*\pi$ invariant mass) and t_{pp} (the proton-to-proton momentum transfer) are plotted for the average transverse momenta as a function of ω. Note that $S_{K^*\pi}$ has a minimum just above $\omega=120°$. In this region the proton has its maximum longitudinal momentum in the backward direction—i.e., the reaction is "most peripheral"—and it is in this vicinity that most of the data points fall. This minimum in $S_{K^*\pi}$ is the location of the Q peak. In Fig. 4(c) is shown the Lorentz-invariant phase-space weight as a function of ω for this reaction. This has two sharp peaks corresponding to configurations in which the pion has zero longitudinal momentum.

In short, if all of the events corresponding to the reaction $K^-p \to K^*\pi p$ had the *same* values of the transverse momenta, then all of the dynamic variables would be functions of the longitudinal momenta alone and would be completely specified by the single parameter ω. As we have seen (Fig. 3) this is very nearly the case for all events in reaction (2), regardless of the mass of the "K^*": The average transverse momenta are essentially the same for all values of the $K^-\pi^+$ mass, and the spread about these average values is very small. With this in mind we use the longitudinal phase-space

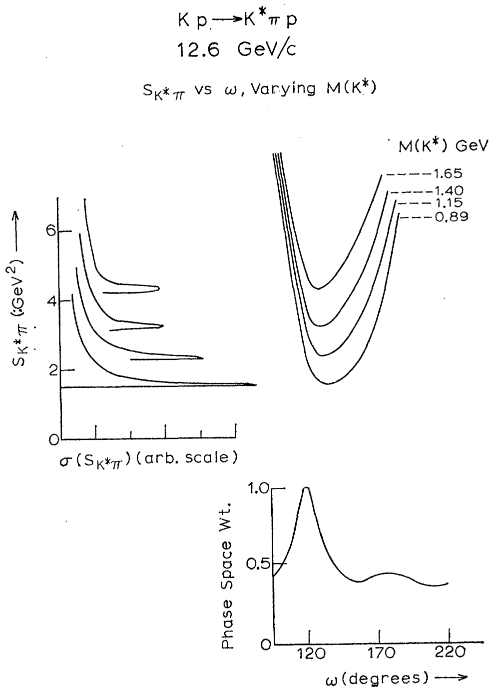

FIG. 5. $S_{K^*\pi}$ versus ω for the reaction $K^-p \to K^*\pi p$ on the interval $100° < \omega < 220°$, showing the effect of varying the K^* mass. Projections are discussed in the text.

picture to investigate the qualitative effects of this behavior on the $K\pi\pi$ mass spectrum. Figure 5 shows curves of $S_{K^*\pi}$ versus ω, in the region of small momentum transfer, for four different values of the $K^-\pi^+$ mass. [Here, and subsequently, we refer to the effective mass of the $K^-\pi^+$ system as $M(K^*)$. This does not necessarily imply a K^* resonance.] The lowest-lying curve in Fig. 5 corresponds to the mass of the $K^*(890)$ resonance and is the same as that shown in Fig. 4(b). The others correspond to successively higher values of the invariant mass of the $K^-\pi^+$ system. Again, each of these curves is calculated for a single set of transverse momenta, the experimental average values.

Each of the four curves in Fig. 5 is shown projected on the $S_{K^*\pi}$ and ω axes assuming that the distributions in the longitudinal momenta are given simply by phase space. Thus the projection on the ω axis is just the phase-space weight, as given in Fig. 4(c). [In principle, there should be four such projections on ω, one for each value of $M(K^*)$. Since these vary only slightly with $M(K^*)$, the average curve is shown.] It will be seen from the projections on the $S_{K^*\pi}$ axis that—for fixed transverse momenta—each K^* mass contributes a sharp threshold peak and a long tail to the $K\pi\pi$ mass spectrum. The effect of the finite widths of the transverse momentum spectra will be to widen these peaks. Thus, given the observed fact that the transverse momenta are restricted to small values, ***phase space alone*** predicts a $K\pi\pi$ spectrum made up of a continuous sequence of

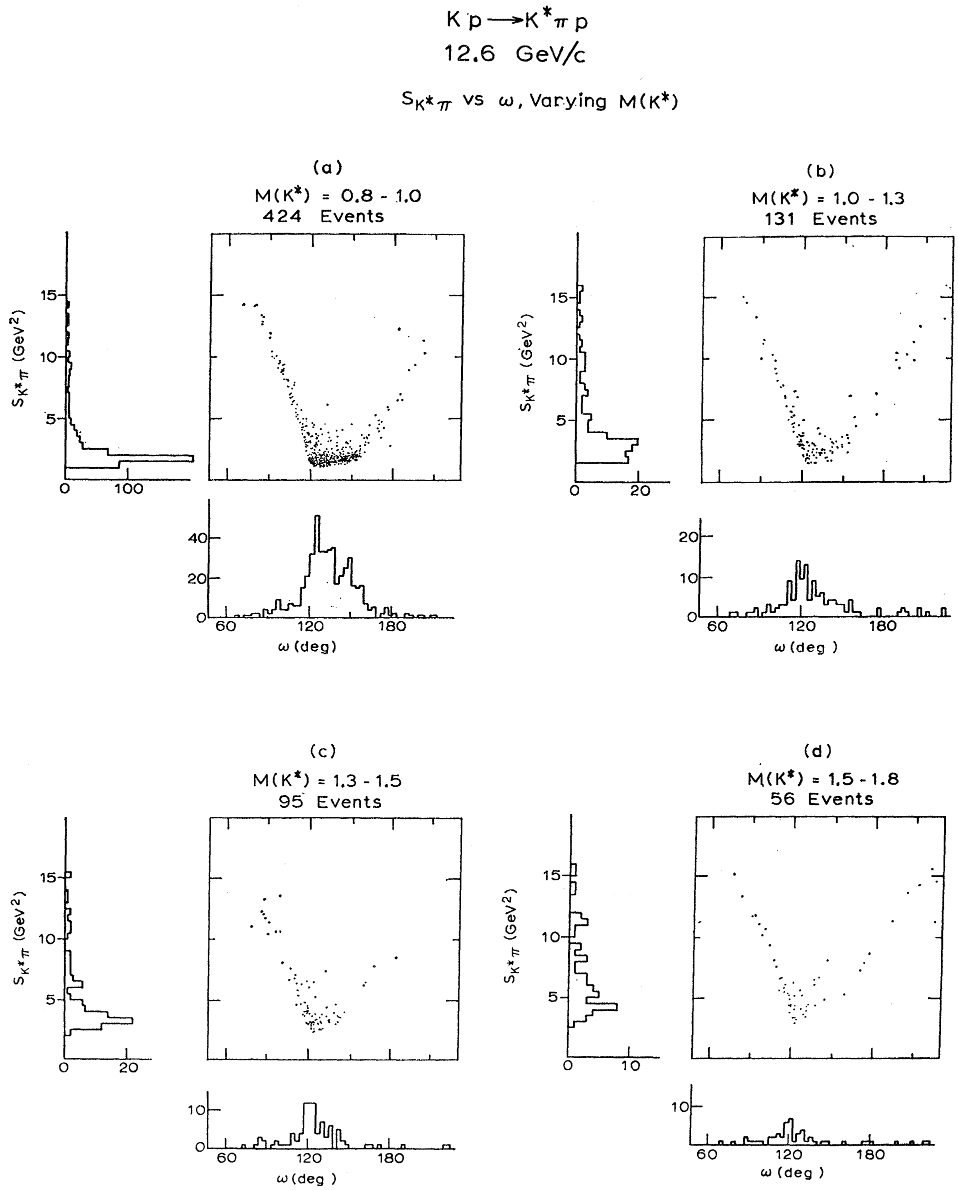

FIG. 6. $S_{K^*\pi}$ versus ω as seen in the data for the reaction $K^- p \to K^* \pi p$, for four selections on $M(K^*)$. These selections are centered on the mass values illustrated in Fig. 5. Δ^{++} background has been removed.

these threshold peaks—a very suggestive result in view of the behavior noted in Sec. I. Furthermore, if there are no additional correlations other than those imposed by phase space, the distribution in ω will be given by the characteristic phase-space shape: a peak centered at $\omega = 120°$.

Figure 6 shows the same distributions, as seen in the data. The square of the $K^*\pi$ mass is plotted versus ω for four different cuts on the K^* mass [i.e., four different cuts on the $K^-\pi^+$ spectrum of Fig. 1(a)].[6] For each slice on the K^* mass a threshold enhancement is seen in $S_{K^*\pi}$. Above the Q peak—Figs. 6(b)–6(d)—the behavior is just as expected for phase space: The points in the scatterplots follow smoothly the average curves shown in Fig. 5, and the distributions in ω have a peak centered at $\omega = 120°$. In the Q region the situation is different. The observed enhancement in $S_{K^*\pi}$ is the result of an intense horizontal band in the scatterplot,

[6] In Figs. 1, 3, 6, and 7 a selection on the $p\pi^+$ invariant mass has been made to remove the $\Delta^{++}(1236)$ background. In the reaction under consideration here, this background contributes significantly at large values of the $K^-\pi^+$ and $K\pi\pi$ masses. In the four regions of the $K^-\pi^+$ spectrum selected in Figs. 6 and 7, the fractions of events removed by this cut are, respectively, 12, 21, 30 and 46%. In the Q peak—the first of these regions—this background is small. Not all of the events removed by this cut are true Δ^{++} signal. In particular, in the Q region, it is judged that removal of these events excludes as much true $K^*(890)$ as true Δ^{++}. Hence in the detailed analysis of the Q region (Sec. III) no cut has been made on the $p\pi^+$ mass. In this case the results obtained were found to be unaffected by the presence or absence of this selection.

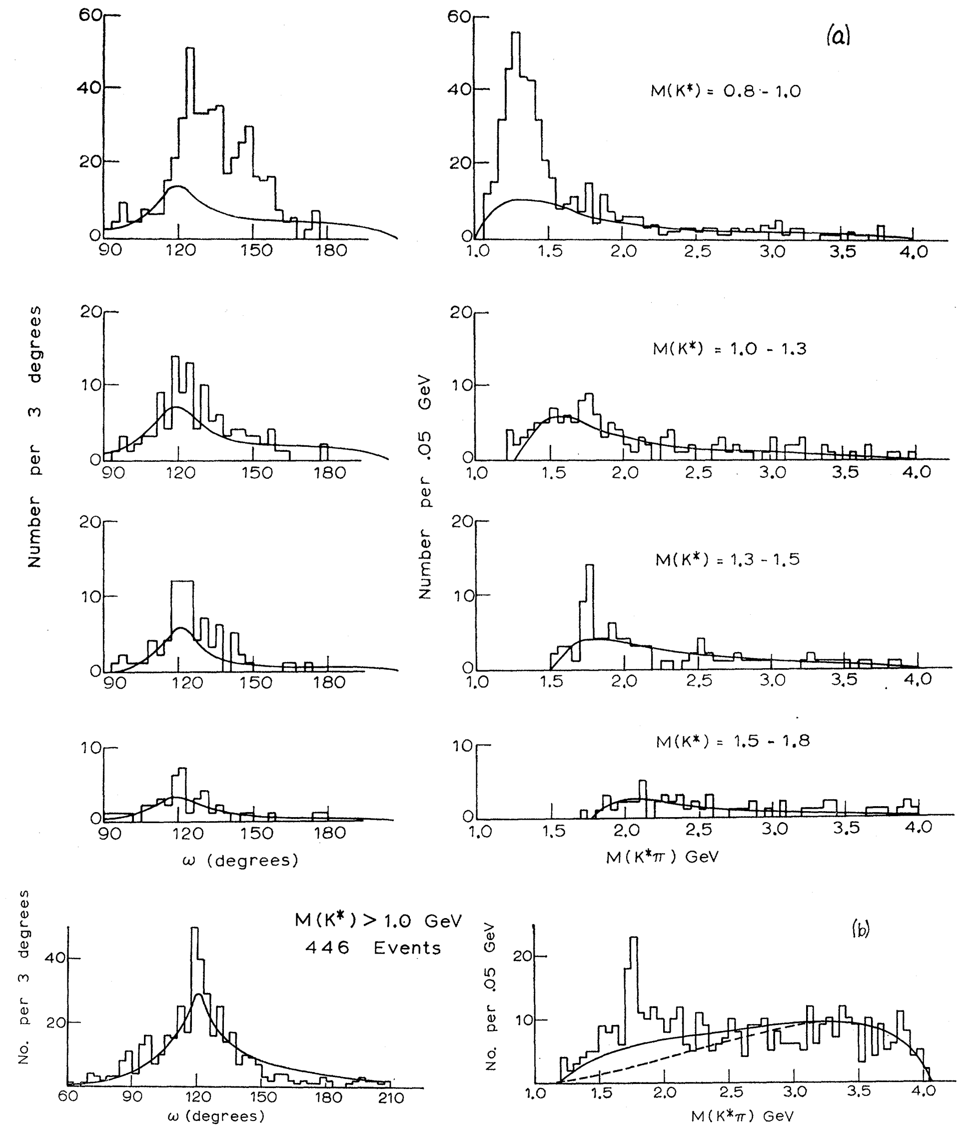

FIG. 7. Distributions in ω and the $K\pi\pi$ invariant mass. Smooth curves are the result of a Monte Carlo calculation in which the following effective matrix element has been imposed on Lorentz-invariant phase space:

$$|M_{\mathrm{eff}}|^2=\exp(at_{pp})\times\exp\{-b[P_t^2(K^*)+P_t^2(\pi^-)+P_t^2(p)]\},$$

where $a=1.5$ (GeV/c)$^{-2}$, $b=4.0$ (GeV/c)$^{-2}$, and the P_t are the transverse momenta. This parametrization gives good agreement with the observed distributions in these variables. In (a) the curves are normalized separately to the data in each interval of $M(K^*)$. In (b) the solid curves, which are arbitrarily normalized to 400 events, include a contribution to the K^* spectrum to account for the tail of the $K^*(890)$ peak (Breit-Wigner shape). The result without this contribution is shown by the dashed curve.

with a resulting distribution in ω which peaks above 120° and has a second peak, or shoulder, at $\omega=150°$. Thus the Q peak exhibits strong correlations between the transverse and longitudinal momenta which are not present elsewhere in the $K\pi\pi$ spectrum.

These results suggest that the observed transverse momentum behavior is indeed of fundamental importance and that, given this behavior, the continuum part of the $K\pi\pi$ spectrum extending above the Q peak in mass, and perhaps including the background beneath the Q, follows from simple phase-space distributions in the longitudinal momenta. This transverse momentum behavior is dynamic in origin, and the restriction to small average values of the transverse momenta is a common feature of all current models of high-energy collisions of hadrons. We do not here speculate on specific models for this behavior, but show in Fig. 7 an attempt to give quantitative substance to the conclusions of the previous paragraphs. Figure 7(a) shows the same data as in Fig. 6, with the same cuts, this time displaying the distributions in ω and the $K^*\pi$ mass (not mass squared). The smooth curves are the result of a Monte Carlo phase-space calculation which includes a peripheral proton and the observed transverse momentum distributions. These curves are seen to describe the data very well, except for the Q peak, and perhaps a small L signal for $1.3<M(K^*)<1.5$ GeV. Figure 7(b) compares this calculation with the data for all events having $M(K^*)$ greater than 1.0 GeV. Here the solid curves were obtained by modifying the calculated K^* mass spectrum to include a contribution from the tail of the $K^*(890)$ signal above $M(K^*)=1.0$ GeV. The result without this modification is shown by the dashed curve in the $K^*\pi$ mass plot.

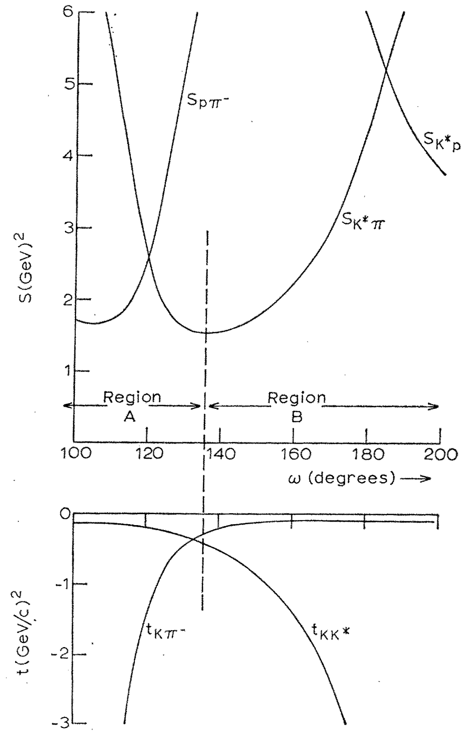

FIG. 8. Two-particle invariant masses and momentum transfers as a function of ω in the Q region, plotted for the average transverse momenta, with $M(K^*)=0.89$ GeV. S_{ab} is the square of the invariant mass of particles a and b. t_{KK^*} and $t_{K\pi}$ are the four-momentum transfers from the incident kaon to the outgoing K^* and π^-, respectively. t_{pp} is nearly independent of ω in this region and is omitted for the sake of clarity [cf. Fig. 4(b)].

Summarizing the results of Sec. II, we find that with the exception of the Q, and perhaps the L, the $K\pi\pi$ mass spectrum can be understood directly in terms of the observed transverse momentum behavior, and can be regarded as a continuous series of rather wide threshold peaks in the $K^*\pi$ mass which are due to the phase-space distribution in the longitudinal momenta. The Q peak cannot be explained by this mechanism alone, but requires additional correlations between the transverse and longitudinal momenta—correlations which should provide sensitive tests when comparing model calculations with the data.

III. Q PEAK: KINEMATIC DUALITY

In this section we apply the techniques developed above to a detailed study of specific models for the production of the Q. We consider only events with $K^*(890)$ in the final state, i.e., the reaction

$$K^-p \to \bar{K}^{*0}(890)\pi^-p\,, \qquad (3)$$

neglecting the smaller contribution from $Q \to K\rho$. The longitudinal phase-space plot for this reaction appears in Fig. 4(a). In Fig. 4(b) we showed curves displaying $S_{K^*\pi}$ and t_{pp} as functions of ω for the experimental average values of the transverse momenta. These curves offer a convenient means of viewing the behavior of the data in such a way that the qualitative effects of small transverse momenta are made clear. In Fig. 8 are shown a more complete set of such curves—on an expanded scale—for the region of phase space occupied by the Q peak. As before, these curves are shown for the experimentally determined average values of the transverse momenta, with $M(K^*)=0.89$ GeV. This picture shows clearly the essentially one-to-one correspondence imposed on the dynamic variables by the fact that the transverse momenta are confined to a narrow range about their average values. Note, in particular, that the locus of $S_{K^*\pi}$ spans two kinematically distinct regions (separated by a dashed line in the figure): Region A ($\omega \lesssim 136°$) is characterized by very small $|t_{KK^*}|$, with rapidly increasing $|t_{K\pi}|$, and vice versa for Region B ($\omega \gtrsim 136°$). The momentum transfers $t_{K\pi}$ and t_{KK^*} are defined in the figure.

We consider first the predictions of a double-Regge-pole-exchange model for reaction (3), taking into account two possible exchange amplitudes.[7] These amplitudes are represented by the diagrams shown in Fig. 9. Diagram A represents the exchange of the pion trajectory between the top and middle vertices and the Pomeranchuk trajectory at the lower vertex. Digram B involves exchange of the $K^*(890)$ and Pomeranchuk trajectories. The parametrization of the model is as follows (M_A and M_B are the invariant amplitudes for the two diagrams; N_A and N_B are normalization constants; unit slopes are chosen for the Regge trajectories α_π and α_{K^*}):

$$M_A = N_A\sigma^+(\alpha_\pi)(S_{K^*\pi}/S_0)^{\alpha_\pi(t_{KK^*})}S_{\pi p}e^{\alpha_{\pi p}t_{pp}/2}\,,$$

$$M_B = N_B\sigma^-(\alpha_{K^*})(S_{K^*\pi}/S_0)^{\alpha_{K^*}(t_{K\pi})}S_{K^*p}e^{\alpha_{K^*p}t_{pp}/2}\,,$$

$$\sigma^+(\alpha_\pi) = \frac{1+e^{-i\pi\alpha_\pi}}{\sin\pi\alpha_\pi}(\alpha_\pi+2)\,,$$

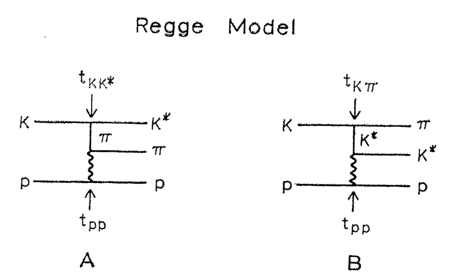

FIG. 9. Double-Regge-pole-exchange-model diagrams.

[7] The application of a multi-Regge model to diffraction-produced threshold enhancements—including the motivation for such an application, which relies heavily on the implications of duality—is discussed in detail by E. L. Berger, Phys. Rev. **179**, 1567 (1969). An earlier analysis of our data in terms of a double-Regge-pole-exchange model, which included only a single diagram (diagram A of Fig. 9) is given in J. Andrews *et al.*, Phys. Rev. Letters **22**, 731 (1969). The calculation employed here follows closely that of M. S. Farber *et al.*, Phys. Rev. Letters **22**, 1394 (1969); and H. Yuta, University of Rochester Report No. UR-875-271, 1969 (unpublished).

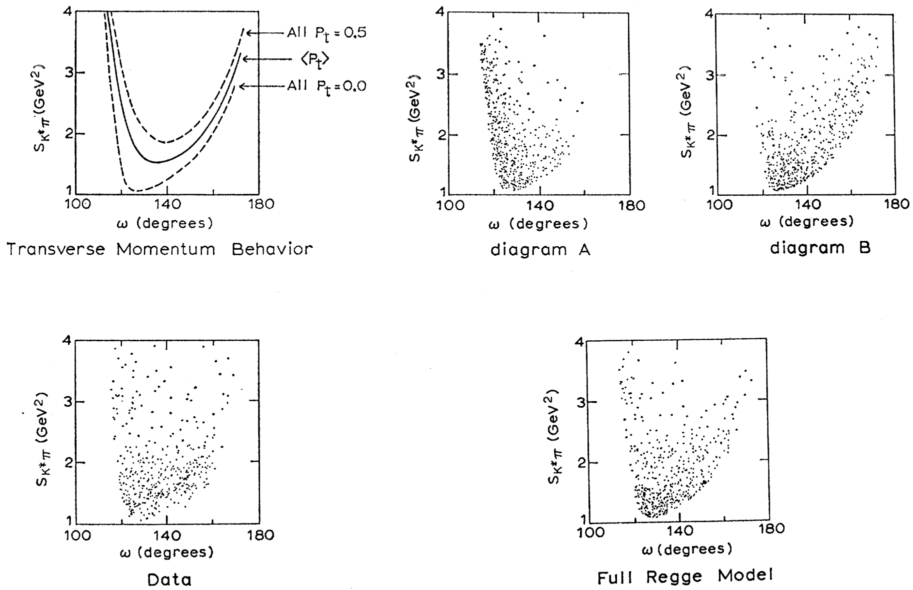

FIG. 10. Regge-model comparison. $S_{K^*\pi}$ versus ω in the Q region. Upper left: effect of varying the transverse momenta. Solid curve is computed for the experimental average values of the transverse momenta. Lower dashed curve is for all transverse momenta equal to zero; the upper curve is for all transverse momenta equal to 0.5 GeV/c. Lower left: the data points (418 events). Right-hand plots show the result of the Regge-model calculation as described in the text. Each of these plots contains 500 Monte-Carlo-generated events.

$$\sigma^-(\alpha_{K^*}) = \frac{1-e^{-i\pi\alpha_{K^*}}}{\sin\pi\alpha_{K^*}}(\alpha_{K^*}+1), \tag{4}$$

$$\alpha_\pi = t_{KK^*} - m_\pi{}^2, \quad \alpha_{K^*} = t_{K\pi} - (m_{K^*}{}^2 - 1),$$

$$S_0 = 1.0 \text{ Gev}^2,$$

$$a_{\pi p} = 7.0 \text{ (Gev}/c)^{-2}, \quad a_{K^*p} = 7.0 \text{ (GeV}/c)^{-2}.$$

Following usual practice, the Pomeranchuk exchange is not explicitly Reggeized, but is approximated by on-mass-shell πp and K^*p elastic diffraction scattering. The diffraction slope $a_{\pi p}$ is chosen to roughly approximate that of π^-p elastic scattering data in the appropriate kinematic range, and the slope $a_{K^*\pi}$, which cannot be obtained from experimental data, is assumed to be the same. The results are not very sensitive to the specific values chosen for these slopes.

No attempt has been made to extract absolute normalizations from the model, as our purpose here is solely to examine the predicted kinematic behavior. In order to do this over as wide a kinematic range as feasible, we have made the cutoff values in t_{KK^*} and $t_{K\pi}$ generously large: $-t_{KK^*}$, $-t_{K\pi}<2.5$ (GeV/c)^2. These cuts exclude no events having $K^*\pi$ mass less than 1.6 GeV. The factors $(\alpha_\pi+2)$ and $(\alpha_{K^*}+1)$ in the signature factors $\sigma^\pm(\alpha)$ are to eliminate unphysical poles in the range of momentum transfers allowed by these cutoffs.

Some qualitative observations regarding this model can be made upon inspection of Fig. 8. We expect diagram A to dominate in Region A, where t_{KK^*} is smallest in magnitude. Similarly, diagram B should represent the dominant amplitude in Region B. Both will contribute heavily near the boundary between these two regions, i.e., near the smallest values of $S_{K^*\pi}$, as here both momentum transfers are small in magnitude.[8] In diagram A the approximation used to parametrize the diffraction scattering of the virtual pion off the target proton is not expected to be valid for small values of $S_{p\pi^-}$, where resonance effects in the $p\pi^-$ system may be important. The same is true of S_{K^*p} in the case of diagram B. From Fig. 8 it can be seen that the exclusion of events with small $S_{p\pi^-}$ (say $S_{p\pi^-}<4.0$ GeV^2) cuts out nearly all of Region A, whereas S_{K^*p} remains large over most of the region of interest. In fact, such a cut on $S_{p\pi^-}$ removes about 20% of the events in the Q peak, whereas no events in this peak have $S_{K^*p}<6.0$ GeV^2. In the discussion which follows, in order to show the behavior of the model as clearly as possible over as wide a range as possible, we will not make a selection on the $p\pi^-$ mass unless specifically noted.

The results of the Regge-model calculation are compared with the data in Fig. 10. These are displayed as scatterplots of $S_{K^*\pi}$ versus ω for values of $S_{K^*\pi}$ near threshold. As emphasized in Sec. II, the interplay between the longitudinal and transverse momenta is important here. The upper left-hand plot in Fig. 10

[8] We note here that the often-used technique of ordering the longitudinal momenta of the outgoing particles to assess the relative importance of various exchange amplitudes is not generally valid when these amplitudes are applied to near-threshold values of one of the two-particle subenergies (e.g., $S_{K^*\pi}$ in the case considered here). As we have pointed out, the two diagrams which we consider are expected to have their respective contributions above and below $\omega \approx 136°$, with considerable overlap between them. The momentum-ordering technique would put this demarcation at $\omega = 150°$, the point at which the K^* and π have equal longitudinal momenta in the forward direction. The difference between these two predictions arises from the difference in the masses of the K^* and π. In fact, neither diagram contributes significantly above $\omega = 150°$, and although the data are best described when the two diagrams contribute in roughly equal amounts, only 15% of the data have $\omega > 150°$.

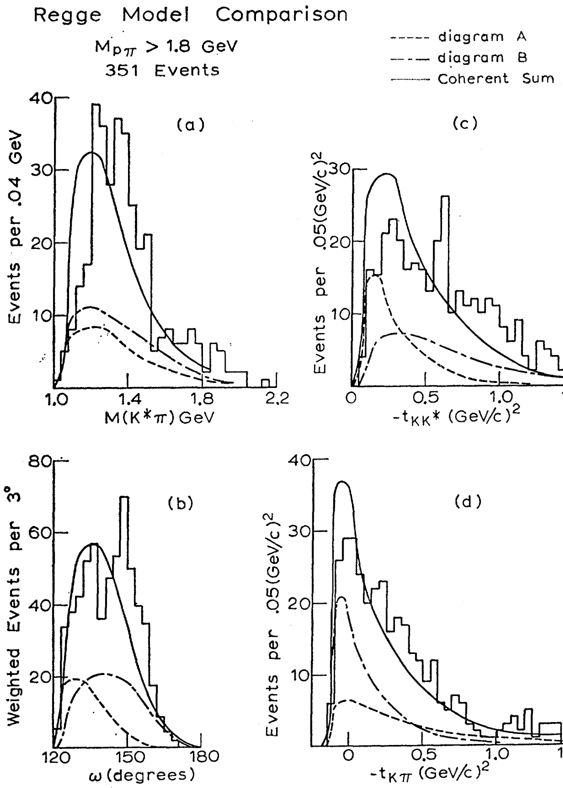

FIG. 11. Comparison of the Regge-model calculation with some projections of the data. Results of including only a single diagram in the amplitude are shown by the broken curves. Solid curves give the result of the coherent sum (see text). Curves as normalized to the data. In (b) each event has been weighted to remove the effects of phase space from the distribution.

shows the locus of $S_{K^*\pi}$ for three different sets of transverse momenta. The plots labeled "diagram A" and "diagram B" contain Monte Carlo events generated according to Lorentz-invariant phase space modified by the squared amplitudes $|M_A|^2$ and $|M_B|^2$, respectively. It will be seen that neither of the two exchange amplitudes gives particularly good agreement with the data. As expected, diagram A contributes most heavily on the left-hand side of the plot (Region A), whereas diagram B favors Region B. Both have their heaviest concentration of points in the lower tip of the allowed phase space, and in this region the kinematic overlap between the two is essentially complete. Away from threshold, each diagram continues to concentrate points near the kinematic boundary—following the small transverse momentum envelope—whereas the data fall off smoothly in $S_{K^*\pi}$, independently of ω. The plot labeled "Full Regge Model" in Fig. 10 shows the result of a coherent sum of the two amplitudes[9]:

$$|M|^2=|M_A+M_B|^2=|M_A|^2+|M_B|^2+2\,\mathrm{Re}M_AM_B. \quad (5)$$

This calculation gives, qualitatively, a more correct description of the data; however, the concentration of points very near threshold in $S_{K^*\pi}$ is not in agreement with the experimentally observed behavior.

Some projections of the data are compared with the model calculation in Fig. 11. Here a cut to exclude small values of the $p\pi^-$ mass has been applied, both to the model and the data. The broken curves show the results for each diagram taken separately; the solid curves are the result of the sum, as given in Eq. (5). In Fig. 11(b) each event has been weighted by the inverse of the Lorentz-invariant phase-space volume element, so that this plot displays directly the effects of the invariant matrix element as a function of the longitudinal phase-space parameter ω. The effects noted in the S-versus-ω plots of Fig. 10 are reflected in Figs. 11(a) and 11(b). In both cases the calculated curves peak at values which are too small to give agreement with the data. In the case of the $K^*\pi$ mass distribution, the model predicts too sharp a rise from threshold, while in the ω distribution the calculated shape peaks too low and is too narrow to account for the behavior of the data near $\omega=150°$.

In summary, if only a single diagram (A or B in Fig. 9) is considered, the double-Regge-pole-exchange model

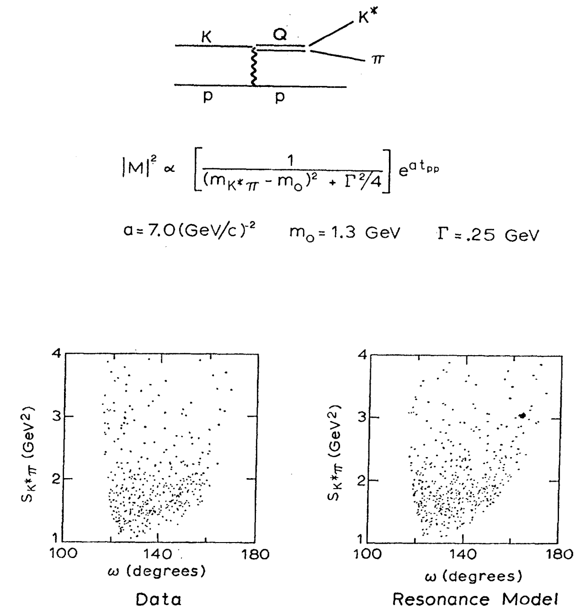

FIG. 12. Resonance model. At the lower left the data are displayed in a scatterplot of $S_{K^*\pi}$ versus ω. Plot on the lower right is the result of the model calculation. This plot includes 500 Monte-Carlo-generated events.

[9] The relative amounts of the two diagrams have been adjusted to give the best fit to the two-particle mass and momentum-transfer distributions. This is obtained when the two diagrams contribute nearly equally. The ratios of the integrated cross sections are diagram A:diagram B:coherent sum=0.3:0.4:1.0. Because of the large overlap between the two, the interference term, which contributes constructively, is equally as important as either of the two constituent amplitudes near threshold in $S_{K^*\pi}$. The relative phase between these amplitudes is given entirely by the signature factors [$\sigma^\pm$ in Eq. (4)]. We have investigated the effect of varying this phase and have not been able to improve the agreement with the data by this means.

appears incapable of giving a correct description of the data except in a very narrow kinematic range (i.e., only if severe momentum-transfer cuts are applied). The two-diagram model reproduces the qualitative behavior but fails to give detailed agreement with the data. This situation might be improved by allowing some of the parameters of the model—such as the slopes of the Regge trajectories and the scale constants—to assume different values from those used here. However, the results are quite insensitive to small changes in these parameters, and large changes from the values chosen would be at variance with Regge-pole fits to two-body processes. At best it must be said that the model does not provide a very natural framework within which to describe the detailed behavior observed in the data.

We now consider another model for the production. It has been found in a number of experiments[10] that

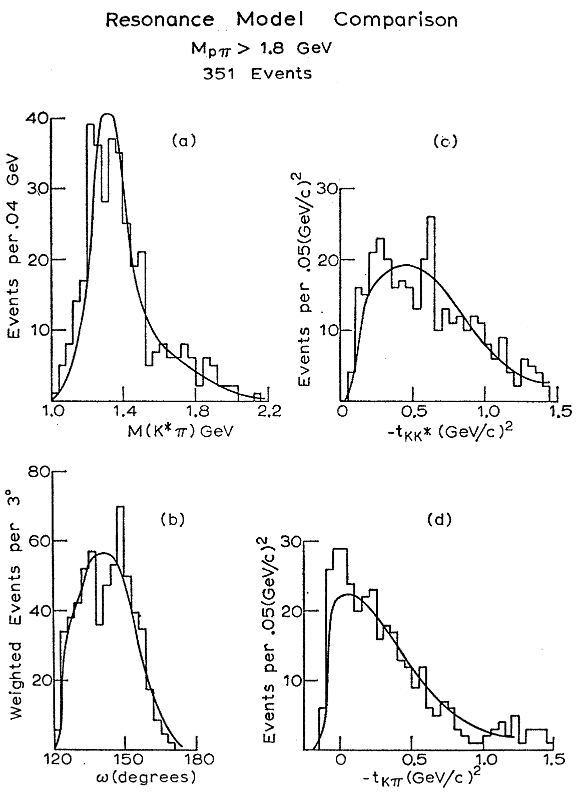

FIG. 13. Comparison of the resonance-model calculation with some projections of the data. Curves are normalized to the data.

[10] The decay characteristics of the Q are treated in detail, using similar analyses, in the following works (in each case the beam momentum and incident particle are given in parentheses): C. Y. Chien *et al.*, Phys. Letters **28B**, 143 (1968) (7-GeV/c K^+); G. Alexander *et al.*, Nucl. Phys. **B13**, 503 (1969) (9-GeV/c K^+); M. S. Farber *et al.*, Phys. Rev. D **1**, 78 (1970) (13-GeV/c K^+); T. Ludlam, Ph.D. thesis, Yale University, 1969 (unpublished) (13-GeV/c K^-). In every case save that of Alexander *et al.*, the results are in agreement with the hypothesis of a single resonance with $J^P=1^+$, and S-wave decay to $K^*(890)\pi$ and $K\rho$. Alexander *et al.* find evidence for two interfering resonances, with $J^P=1^+$, in the Q region.

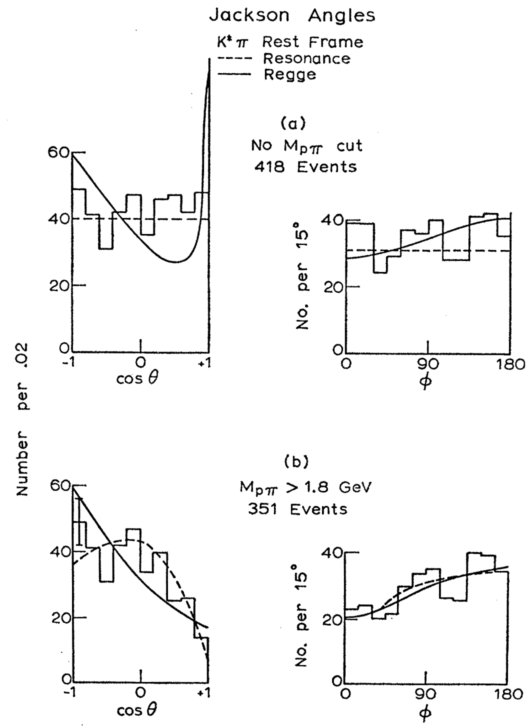

FIG. 14. Polar and azimuthal angles of the $K^*(890)$ in the Jackson frame ($K^*\pi$ rest system):

$$\cos\theta = \hat{p}_K \cdot \hat{p}_{K^*},$$

$$\cos\phi = [(\mathbf{p}_K \times \mathbf{p}_{K^*}) \cdot (\mathbf{p}_T \times \mathbf{p}_p)] / |\mathbf{p}_K \times \mathbf{p}_{K^*}|\,|\mathbf{p}_T \times \mathbf{p}_p|,$$

where $\mathbf{p}_K$ and $\mathbf{p}_T$ are the momentum vectors of the incident kaon and target proton, respectively. Solid curves are the result of the Regge-model calculation (coherent sum of diagrams A and B); the broken curves are the result of the resonance-model calculation. Curves are normalized to the data.

the angular correlations among the momenta for events in the Q peak are consistent with the decay of a single resonant state having spin and parity 1^+. These investigations have been performed in such a way as to be uncoupled from the effects of the production mechanism. We show here, for comparison with the foregoing results, the predictions of a very simple model for the production of such a resonance in the $K^*\pi$ system of reaction (3). The model is shown in Fig. 12. We take for the invariant amplitude an S-wave Breit-Wigner shape in the $K^*\pi$ mass, produced with an exponential dependence on the proton-to-proton momentum transfer. The parameters m_0 and Γ were chosen to approximate closely the position and width of the Q peak. The exponential slope in t_{pp} is the same as was employed for the Regge model. No background is included.

As before, a Monte Carlo calculation was performed for comparison with the data. This comparison is shown in the lower part of Fig. 12, and in Fig. 13. The same momentum-transfer cuts were applied as with the Regge model. In Fig. 13 a cut on the $p\pi^-$ mass was made in order to make these results directly comparable with those of Fig. 11. (The histogrammed data are identical in these two figures). The agreement with the data is quite remarkable. Particularly noteworthy is the superiority of this crude resonance model over the Regge model in reproducing the weighted ω distribution [compare Figs. 11(b) and 13(b)]. As a further comparison of the two models with the data, we show in Fig. 14 the polar and azimuthal Jackson angles for the K^*, in the $K^*\pi$ rest frame, with and without the cut on $p\pi^-$ mass. Note that without this selection the data are completely consistent with the isotropic predictions of the S-wave resonance. The Regge model is incompatible with this behavior. Both models give reasonable agreement with the distributions obtained when small $p\pi^-$ mass values are excluded.

These results would seem to support the view that the Q peak is predominantly the result of a resonant state. They are also in complete accord with the concept of duality: If we look to detailed comparisons of finite-energy sum rule predictions with two-body scattering data (see, for instance, Ref. 2) we find that whereas a Regge-pole form often gives a very good *average* description of low-energy, resonance-dominated amplitudes, adequate *local* descriptions of these amplitudes are not obtained for cases in which a single resonance dominates near threshold. We point out, however, that another sort of duality is apparent in this analysis. This is a kinematic duality. Both of the models discussed here for the production of the Q have a built-in exponential damping in the proton-to-proton momentum transfer [$\exp(at_{pp})$]. Furthermore, both models (and any model worthy of serious consideration) can reproduce, in some sense, the threshold peak in the $K^*\pi$ mass spectrum. These two features are sufficient to guarantee that all of the outgoing particles will have small transverse momenta, with the result that the dynamic variables will be restricted to very narrow bands of phase space following curves such as those shown in Fig. 8. Hence all such models can be expected to give qualitatively similar results, at least over a limited range in the momentum transfers. Our resonance model includes *only* these two features. This model cannot be regarded as a complete description of the Q. It does not, for instance, reproduce one of the best known features of diffraction-produced quasi-three-body-final states: that the observed forward peak in the momentum-transfer distribution, $d\sigma/dt_{pp}$, has an exponential slope whose value is strongly dependent on the mass of the produced system.[11] The Regge model does give this behavior (as pointed out by Berger[7]), while the resonance model simply reproduces the input slope.

Thus the comparison between the two models discussed here, rather than providing a definitive conclusion as to the nature of the Q peak, illustrates the following points: (i) that the resonance model appears to give a more natural description of the data than does the Regge-pole model, and (ii) that the qualitative similarities between the detailed predictions of these models can be understood solely on the basis of kinematics.

ACKNOWLEDGMENTS

We thank Dr. John Andrews and Dr. Joseph Lach for their essential contributions during the earlier stages of this experiment. Thanks are also due to Mr. Marvin Johnson and to Dr. Dixon Bogert and Dr. Horace Taft for their assistance. We have enjoyed useful discussions with Dr. Richard Slansky and with Dr. Thomas Ferbel and his co-workers. We gratefully acknowledge the excellent help of the staffs of the Brookhaven National Laboratory Alternating Gradient Synchrotron and 80-in. bubble-chamber facilities, and of the Yale scanning and measuring staff.

[11] See, for instance, J. Bartsch *et al.*, Phys. Letters **27B**, 336 (1968); B. Y. Oh and W. D. Walker, *ibid.* **28B**, 564 (1969).